Systematic Analysis and Design of Single-Phase Boost PFC Converter for Induction Motor Drive

Dr. Jafar H. Alwash
Engineering College, University of Baghdad/ Baghdad
Email: jalwash@yahoo.com
Dr. Turki K. Hassan
Engineering College, University of Al-Mustansiriyah / Baghdad
Raed F. Abbas
Engineering College, University of Baghdad/ Baghdad

Received on: 8/72013 & Accepted on: 6/2/2014

ABSTRACT

This paper presents a systematic analysis and design of a single-phase boost power factor correction (PFC) converter supplying an inverter-motor drive system. The PFC converter is a single-stage single-switch boost converter that uses a current shaping technique to reshape the non-sinusoidal input current drawn by the motor-drive system to a near sinusoidal waveform. The resultant is a current input with almost free-harmonics, which comply with the IEC 61000-3-2 limits, and a system operates with near unity power factor. The other function of the boost converter is to provide a regulated DC voltage to the inverter-motor system. The motor drive system incorporates a1-hp induction motor fed by a Pulse Width Modulation (PWM) inverter with open-loop voltage to frequency (v/f) control. This drive system is analyzed as a load across the converter and its equivalent resistance is extracted and used in the PFC controller design. The theoretical and experimental results are compared to validate the analysis.

Keywords :Index Terms—Boost converter, power factor correction, induction motor, equivalent resistance.

تحليل وتصميم محول رافع احادي الطور ذو معامل قدرة مصحَح لسواقة المحرك الحثي

الخلاصة: يقدم هذا البحث تحليل منهجي وتصميم محول رافع احادي الطور ذو تقنية تصحيح معامل القدرة يُجهّزُ نظامَ مكون من عاكس (inverter) ومحرّك حثي. مصحح معاملَ القدرة هو محول رافع ذو مرحلةٍ واحدة ومفتاحٍ واحد يستخدم تقنية تشكيل التيار ليعيد تشكيل تيار الدخل اللاجيبي المسحوب من قبل نظام العاكس\المحرك الى تيار جيبي تقريبا. باستخدام هذه التقنية سيتم الحصول على تيار دخل خالٍ من التوافقياتِ تقريباً يلتزم بالمواصفات القياسية (IEC 61000-3-2)، بالإضافة الى الحصول على نظام يعمل بمعاملِ قدرة قريب من الواحد. الوظيفة الأخرى للمحول الرافع هي تزويّدَ نظام العاكس\المحرك بفولتية مستمرة (DC) منظمة. يتألف نظام العاكس\المحرك من محرك حثي ثلاثي الطور وعاكس مضمن بطريقة عرض النبضة يعمل

https://doi.org/10.30684/etj.32.7A13
2412-0758/University of Technology-Iraq, Baghdad, Iraq

بتقنية ثبوت نسبة الفولتية الى نسبة التردد (v/f) باستخدام سيطرة الحلقة المفتوحة. تم تحليل هذا النظام كحمل عبر المحول الرافع وذلك بحساب مقاومته المكافئةِ لكي تستخدم عند تصميمِ جهازِ سيطرة المحول .تم مقارنة النتائج النظرية والتجريبية للتحقق من صحة التحليل.

INTRODUCTION

Most industrial applications utilize induction motors as variable speed drives such as inverter-fed variable-voltage variable-frequency and field-oriented controlled ac motor drives. Consequently, the traditional rectifiers, which are largely used to provide dc source for these drives, cause significant harmonic problem and poor power quality due to the nonlinearity of the diode rectifier and the capacitive filter (between the rectifier and the inverter). This behavior causes non-sinusoidal input ac currents leading to inject harmonics into the utility lines and thus producing a current distortion. These effects draw the system performance to a low power factor and reduce the maximum power available from the power lines and so reducing the efficiency.

Recently, Power Factor Correction (PFC) converters have been used in these drive systems to improve the power factor of the input current waveform and to meet the requirement of international standards such as IEC 61000-3-2 [1]. On the other hand, these converters are responsible for regulating the DC bus voltage supplied to the inverter-motor stage. The converter-inverter systems for motor drives have been covered in the literature with different topologies [2-7] and an input utility with nearly unity power factor and low harmonic distortion are obtained. However, most of the work dealt with PFC for motor drive focus on the inverter-stage and its control scheme [8-12] while the PFC control has not been very much studied. Specifically, the behavior of the inverter-motor stage as a load across the PFC converter has not been clarified. This issue was first reported by Bellar*et al.* [13] and later addressed by Chai and Liaw [14] but without any analysis.

A typical single-phase PFC converter fed three-phase motor drive system shown in Fig.1 comprises of input voltage rectified circuit, boost PFC converter, and inverter-motor stage. The output voltage of the boost converter is a DC voltage (with insignificant 2nd-order harmonic ripple). This DC voltage is supplied to the inverter-motor drive system, which is considered as a variable load; accordingly, this variable load is seen by the boost converter as a variable resistive load. It will be shown, in section 3, that in order to design the PFC controller, this variable resistive load should be known. To do so, the inverter-motor system was analyzed to understand its behavior and to extract its equivalent resistance that is seen by the converter. This issue has never been discussed in the reviewed literature concerning the PFC for motor drives system. Therefore, verifying this issue represent an object in this paper.

The first function of PFC converter is to eliminate the harmonics content in the input current and ensure high power factor. Boost converter operated in Continuous Conduction Mode (CCM) is the most frequently form of a PFC converter [15-17], and the Average Current Control (ACC) is the common technique used in PFC converter which incorporates two loops (inner current loop and outer voltage loop). Usually, a current error amplifier, which is a two-pole, one-zero compensation network, is used in the inner loop which increases the complexity in control system. Furthermore, a systematic derivation procedure for both control loops (inner and outer loops) is still missing and this necessitates the use of trial-and-error procedures in the design of the control parameters [15]. The derivation procedure proposed by Chu et al. [15] results in a complex control circuit due to the existence of the current

reference differentiator and the use of four sensing circuit instead of three as in ACC technique. Another category is reported in the development of the current mode technique, which is the feedforward control [18-21]. Basically, the objective of this technique is to generate a nominal duty ratio pattern in order to ease the task of the feedback controller. All the previous mentioned works used a digital controller to implement the feedforward controller.

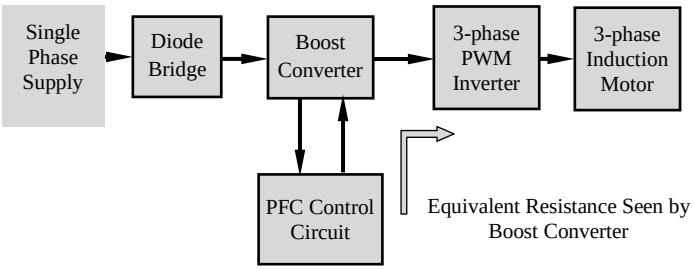

Figure.(1) Block diagram of boost PFC converter fed induction motor

The PFC converter is often ended with an output capacitor to provide a good regulated DC voltage. This is the second function of the PFC converter achieved through the outer voltage loop. The design of the outer loop in a single stage converter topology is difficult due to the presence of a relatively high ripple with twice the line frequency on the output voltage. This voltage ripple causes a considerable distortion in the reference current generated by the voltage loop, which in turn distorts the input current. However, if the output capacitor is relatively high and the voltage controller is designed with a low bandwidth the input current distortion is nearly disappeared. A poor dynamic response is the result of this approach, in other words, the output voltage would have a slow transient response with a relatively large overshoot that may add more stress on the circuit components. Many approaches have been reported in the literature to improve the transient response but at the expense of harmonic reduction, cost, complicated control circuit, or narrow load ranges. In fact, with a single stage PFC converter, it is difficult and nearly impracticable to achieve good dynamic response (good voltage regulation) and minimum input current distortion (good PFC) at the same time [22]. This is because there is an inherent trade-off between output voltage dynamic and input current distortion in the single stage converter.

In this paper, a simplified version of the feedforward controller presented in [19] is used that it can be easily implemented with analogue circuit. The effect of input voltage variation can be removed from the current control loop by introducing the feedforward signal and then a simple proportional (P-controller) is used in the feedback control loop. A Proportional-Integral (PI) controller is used in the outer loop with relatively low bandwidth, to eliminate the voltage ripples. The complete control system is designed and implemented with analogue circuit devices.

SYSTEM CONFIGURATION AND MODEL

Operation Principle of Boost PFC Converter:

Single-phase single-switch boost PFC circuit consists of a main power circuit and a control circuit as shown in Fig.(2). The power circuit mainly comprises of a

full-bridge diode rectifier circuit followed by a boost dc-dc converter and a capacitor filter. A well-designed controller that controls the main switch in the converter can perform a unity power factor correction and output voltage regulation. PFC converter utilizes two-loop control structure; with an outer voltage-regulating control loop providing reference to an inner current-shaping loop.

Through the action of the inner loop controller, the inductor current is constrained to follow the rectified input voltage, resulting in a nearly sinusoidal input current waveform. According to the conventional structure of feedback control system shown in Fig.(3), the voltage controller (G_{cv}) in the outer loop is used to regulate the error signal (v_{err}) and produce the control signal (v_{iL}). By multiplying v_{iL} with the rectified sine wave (v_{rec}) a current reference i_{ref} is yielded. Then, the switching control is obtained by comparing the current controller (G_{ci}) output, which is denoted by (v_{cont}), with a fixed frequency triangular wave (v_{tri}) through a PWM comparator to achieve the input current shaping.

To simplify the analysis of the converter for high PF operation with low line current total harmonic distortion, the following assumptions are made:

- The power switch and the diode are ideal switches and the switching losses are neglected.
- Parasitic components of the inductor and the output capacitor are neglected.

Inner Current Control Loop

In the current control scheme shown in Fig. (4), the feedback controller (G_{ib}) is augmented with a command feedforward controller (G_{iff}) which is used to reduce the command tracking error. Considering that the converter is operated in CCM and the output voltage is ripple-free due to the sufficiently large capacitor C_o, and well regulated such that it is assumed equal to the voltage reference V_{ref}, the differentialequation (1) which represents the state space average model of the power stage may be expressed as [15]

$$L\frac{di_L}{dt} = v_{rec} - (1-d)V_{ref} \quad \ldots(1)$$

According to Fig.4, the duty ratio $d$can be expressed as

$$d = \frac{v_{cont}}{V_{tri}} = \frac{v_{contb} + v_{contff}}{V_{tri}} \quad \ldots(2)$$

where V_{tri} is the amplitude of the sawtooth signal and $1/V_{tri}$ is the gain of PWM unit.

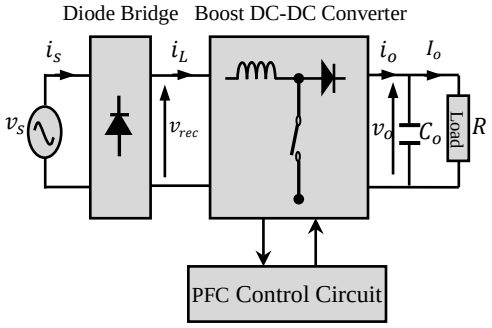

Figure.(2) Block diagram of boost PFC

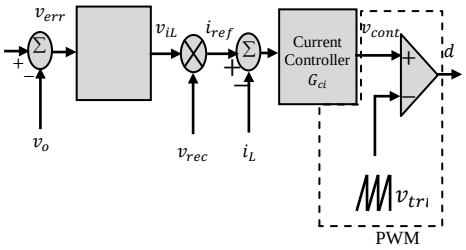

Figure.(3) Control scheme of the converter

The command feedforward control (v_{contff}) can be given as [19]

$$v_{contff} = V_{tri}\left(1 - \frac{v_{rec}}{V_{ref}}\right) \quad \text{... (3)}$$

By substituting (2) and (3) into (1), the inductor current equation will be simply given as

$$\frac{di_L}{dt} = \frac{V_{ref}}{LV_{tri}} v_{contb} \quad \text{... (4)}$$

Due to the linear nature, equation (4) can be expressed in the s-domain as:

$$i_L(s) = \frac{V_{ref}}{sLV_{tri}} v_{contb} \quad \text{... (5)}$$

Equation (5) shows that the effect of input voltage variation in the average model of the power stage (equation (1)) had been removed by introducing the feedforward signal v_{contff} in the control loop. Further-more, the equivalent plant model in the Fig.5 is a first-order model. This means that a simple Proportion-type (P-controller) can be used in the current controller, that is, $G_{ib}(s) = k_{pi}$ where k_{pi} denotes the proportional gain.

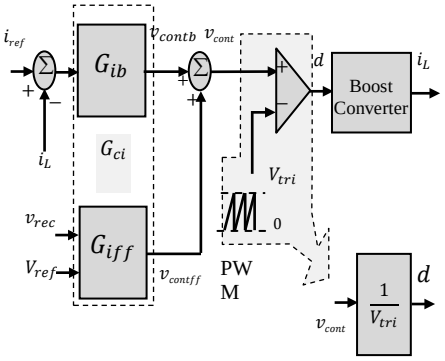

Figure.(4) Current control scheme [19]

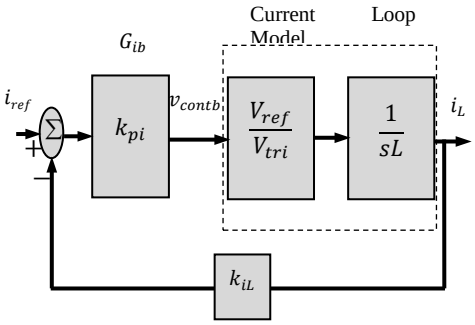

Figure.(5) Equivalent current-loop control [19]

From Fig.(5), the open loop $G_{iOL}(s)$ and closed loop $G_{iCL}(s)$ transfer functions can be expressed as

$$G_{iOL}(s) = \frac{k_{iL}k_{pi}V_{ref}}{LV_{tri}s} \quad \text{... (6)}$$

$$G_{iCL}(s) = \frac{i_L(s)}{i_{ref}(s)} = \frac{k_{pi}V_{ref}}{LV_{tri}s + k_{iL}k_{pi}V_{ref}} \quad \text{... (7)}$$

where k_{iL} denote the sensing gain of the inductor current.

Outer Voltage Control Loop:

A simple proportional-plus-integral (PI) type controller is used to control the outer voltage loop. The dc side capacitor voltage (v_o) is fed back and compared with a control reference, and the error v_{err} is compensated by the PI-controller to produce v_{iL} which in turn provides the reference current to the inner-loop through multiplying it by a rectified

sine wave signal $s(t)$ as shown in Fig.6. The transfer function of the PI-controller can be expressed as

$$G_{cv}(s) = k_p + \frac{k_i}{s} = k_p \frac{s + \omega_z}{s} \quad \ldots (8)$$

where k_p and k_i are the proportional and integral gains, respectively, ω_z is the angular frequency of the zero in the PI controller and $\omega_z = k_i/k_p$.

To design the outer loop controller, the inner loop is considered as a unity gain block; the inductor current i_L has tracked the reference current i_{ref}, as illustrated in Fig.(6). Then, referring to Fig.(7), the open loop transfer function of the outer loop $G_{vOL}(s)$ can be expressed as

$$G_{vOL}(s) = G_{cv}(s) G_{pv}(s) k_{vo} \quad \ldots (9)$$

The small signal control-to-output voltage transfer function ($G_{pv}(s)$) which can be used to design the voltage loop is expressed as [25]

$$G_{pv}(s) = \frac{\hat{v}_o(s)}{\hat{v}_{iL}(s)} = \frac{k_{vi} k_f^2}{k_{Vff}^2 k_{iL} V_o} \frac{R}{2 + RC_o s} \quad \ldots (10)$$

Now, substituting (8) and (10) into (9) yields

$$G_{vOL}(s) = \frac{k_{vi} k_f^2 k_{vo}}{k_{Vff}^2 k_{iL} V_o} \frac{R_{eq} k_p (s + \omega_z)}{R_{eq} C_o s^2 + 2s} \quad \ldots (11)$$

where k_{vi}, k_{vo}, k_{Vff} denote the scaling factors of the rectified input voltage, output voltage, and the input voltage feedforward respectively. The load R is replaced by (R_{eq}) which denotes the equivalent resistance of the inverter-motor system that will be derived in section 3. k_f denotes the form factor (rms/average) of the full wave rectified voltage which is equal to 1.11 ($\pi/2\sqrt{2}$) and expressed as

$$k_f = \frac{V_{rms}}{V_{ff}} \quad \ldots (12)$$

where V_{rms} is the rms of the input supply, V_{ff} is the output signal of the input voltage feedforward circuit which represents the average of the rectified input voltage. This feedforward voltage is essential to remove the effect of input voltage variation by generating a rectified sine wave signal $s(t)$ [23].

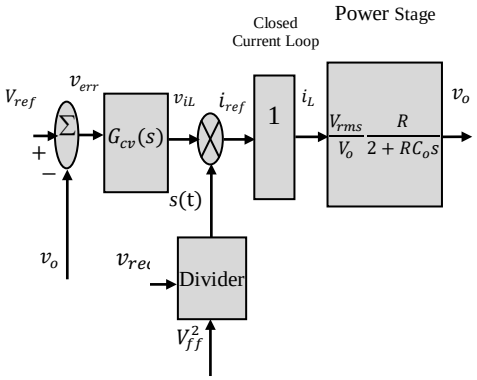

Figure.(6) Voltage control scheme

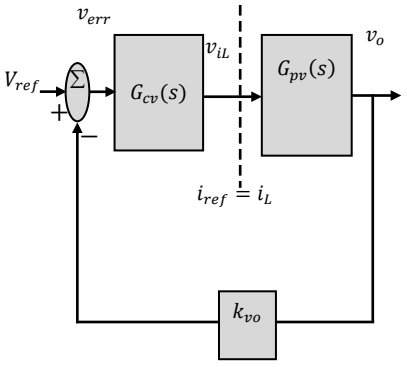

Figure.(7) Block diagram of the voltage loop

PFC Converter Fed Induction Motor Drive

As illustrated in Fig. 1, the PWM inverter with open loop constant voltage to frequency (v/f) control is feeding the three-phase induction motor as a variable speed drive. The inverter-motor drive system is connected to the DC-link of boost converter. Since the inverter-motor drive system is supplied by a DC voltage via the boost converter with negligible output voltage ripple, the drive system is drawing DC current. Accordingly, the equivalent load represented by this system that seen by the converter is considered as an equivalent resistive load. The objective here is to analyze the inverter-motor system and find this equivalent resistance. This may be done by reflecting the motor equivalent impedance through the inverter and back to the converter.

Input Power Equation: The stator active input power is given as [26]

$$P_{in} = 3V_{in}|I_1|cos\varphi_1 \quad \text{... (13)}$$

where V_{in} denote the rms phase voltage input to the motor and φ_1 is the angle between input voltage V_{in} and the input current I_1.

Depending on The approximate per-phase equivalent circuit of three-phase induction motor at steady state operation, the input power can be rewritten as [25]

$$P_{in} = 3V_{in}^2 \frac{r_{12s}}{(r_{12s}^2 + x_{12}^2)} \quad \text{... (14)}$$

where r_{12s} and x_{12} represent $(r_1 + r_{2s})$ and $(x_1 + \acute{x}_2)$ respectively; r_1 and x_1 are the stator resistance and reactance respectively, ($r_{2s} = \acute{r}_2/S$, where S is the motor slip) and $\acute{x}_2$ represent the rotor equivalent resistance and reactance referred to the stator respectively.

It should be noted that the magnetizing resistance (r_m) is not considered in equation (14). Now, the input power can be derived taking r_m into account to be as follows [25]

$$P_{in} = 3V_{in}^2 \frac{r_{12s}^2 + x_{12}^2 + r_{12s}r_m}{r_m(r_{12s}^2 + x_{12}^2)} \quad \text{... (15)}$$

Reflection through PWM Inverter: The typical PWM inverters employing triangular-sinewave modulation drive the switching signals through comparing a sinusoidal reference signal with a high frequency triangle wave signal. The rms value of output fundamental line to line voltage of the PWM inverter is expressed as follows [8]

$$V_{L-L} = \frac{\sqrt{3}m}{2\sqrt{2}} V_{dc} \quad \text{... (16)}$$

where V_{dc} is the inverter DC bus voltage which represents the output voltage of the boost converter (V_o), and m is the modulation index ($0 < m < 1$).

Now, for delta-connected induction motor, the line to line output voltage of the PWM inverter represents the input voltage to the motor, i.e. $V_{L-L} = V_{in}$, then

$$V_{in} = \frac{\sqrt{3}m}{2\sqrt{2}} V_{dc} \quad \text{.... (17)}$$

Substituting (17) into (14), we get:

$$P_{in} = \frac{9\,m^2}{8} V_{dc}^2 \frac{r_{12s}}{(r_{12s}^2 + x_{12}^2)} \quad \ldots.(18)$$

V/F Control Technique: This technique depends on supplying a constant ratio of magnitude and frequency of the stator voltage in an AC motor drive system. To validate this, usually the following assumptions are required:

- The voltage applied to the three-phase induction motor is sinusoidal.
- The voltage drop across the stator resistance is small compared to the stator voltage.

Then, at steady state,

$$\psi_s \approx \frac{V_{in}}{\omega} = \frac{V_{in}}{2\pi f_{inv}} \quad \ldots (19)$$

where ψ_s denotes the stator flux linkage, ω is the angular frequency, and f_{inv} is the fundamental frequency of the PWM inverter. Accordingly, for obtaining a constant flux, the stator voltage should be adjusted in proportion to the supply frequency, then:

$$\frac{V_{in}}{f_{inv}} = k \quad \ldots (20)$$

For variable speed operation, the typical torque slip characteristic for three-phase induction motor under a constant load torque, with negligible mechanical losses, is given in Fig. 8. In this situation, the supply voltage is not constant, but is varied in proportion to frequency in order to keep the motor magnetic flux constant at its rated value. The rotor slip and speed change as the frequency changes. The synchronous and rotor speeds at the reduced frequencies are ω_{si} and ω_{ri} respectively, where i is an integer number. From Fig. (8), one can say that $(\omega_{si} - \omega_{ri})$ is remaining nearly constant as the frequency changes. This may be valid approximation if one assumes that the torque-slip characteristics are linear within the constant load range and remain with the same slope when the slip is changed. Then,

$$K_{\omega i} = \omega_{si} - \omega_{ri} \quad \ldots (21)$$

where $K_{\omega 1} = K_{\omega 2} = K_{\omega i} = K_{\omega}$, and K_{ω} is a constant.

Substituting (21) in the slip-speed relationship, yields:

$$S = \frac{\omega_s - \omega_r}{\omega_s} = \frac{K_{\omega}}{\omega_s} = \frac{K_{\omega}}{2\pi f_{inv}/p_p} \quad \ldots (22)$$

where p_p denotes the pole-pairs of the induction motor.

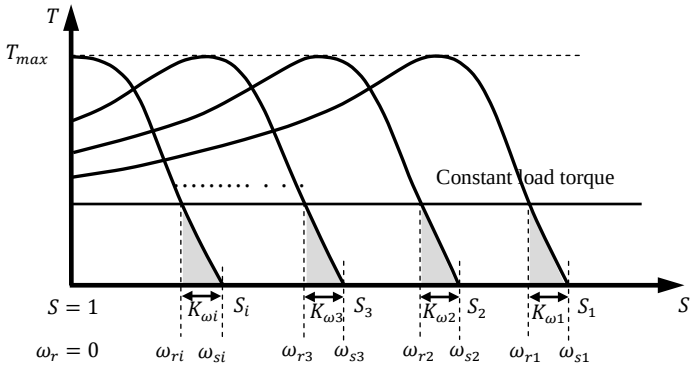

Figure. (8) Torque-slip characteristics for variable speed operation [27]

To find a relation between the modulation index and slip, the frequency of the inverter f_{inv} in equation (22) should be replaced using equation (20):

$$S = \frac{K_\omega}{2\pi V_{in}/p_p k} \quad \ldots (23)$$

By using (17) and (23), the modulation index can be expressed as:

$$m = \frac{\sqrt{2}\, p_p k K_\omega}{\sqrt{3}\pi V_{dc} S} \quad \ldots (24)$$

By substituting equation (24) into the input power equation (18), yields:

$$P_{in} = \frac{3}{4}\left(\frac{p_p k K_\omega}{\pi S}\right)^2 \frac{r_{12s}}{(r_{12s}^2 + x_{12}^2)} \quad \ldots (25)$$

where P_{in} represents the input power to the motor or the output power of the inverter. The efficiency of the inverter can be expressed as:

$$\eta_{inv} = \frac{P_{in}}{P_{dc}} \quad \ldots (26)$$

where P_{dc} is the DC input power to the inverter-motor system which represents the output power of the boost PFC stage (P_o), and can be expressed as

$$P_{dc} = P_o = V_o I_o \quad \ldots (27)$$

where I_o denotes the dc output current.
Then, by substitute (25) and (27) into (26), we get:

$$V_o I_o \eta_{inv} = \frac{3}{4}\left(\frac{p_p k K_\omega}{\pi S}\right)^2 \frac{r_{12s}}{(r_{12s}^2 + x_{12}^2)} \quad \ldots (28)$$

Then, equation (28) may be rearranged to be equivalent to the DC current which has been drawn by the inverter-motor system as follows:

$$I_o = \frac{V_o}{R_{eq}} = \frac{3}{4\eta_{inv}}\left(\frac{p_p k K_\omega}{\pi V_o}\right)^2 V_o \frac{r_{12s}}{S^2(r_{12s}^2 + x_{12}^2)} = \frac{k_s V_o}{\eta_{inv}} \frac{r_{12s}}{S^2(r_{12s}^2 + x_{12}^2)} \quad \ldots (29)$$

where k_s is a constant and given as: $k_s = \frac{3}{4}\left(\frac{p_p k K_\omega}{\pi V_o}\right)^2$

From equation (29), one can simply extract the equivalent resistance that is seen by the converter to be as:

$$R_{eq} = \frac{S^2(r_{12s}^2 + x_{12}^2)}{k_s r_{12s}} \eta_{inv} \quad \ldots (30)$$

Then, with negligible losses in the inverter, then

$$R_{eq} = \frac{S^2(r_{12s}^2 + x_{12}^2)}{k_s r_{12s}} \quad \ldots (31)$$

The equivalent resistance expressed by equation (31) is dependent on two variables: the slip and the reactance of the induction motor. In general, any reactance (x) in the induction motor is expressed as (note that the supply frequency is here the frequency of the inverter):

$$x = 2\pi f_{inv} L \quad \ldots \quad (32)$$

Then, using (22), equation (32) becomes:

$$x = \frac{K_\omega}{S/p_p} L \quad \ldots (33)$$

Equation (33) shows that all the reactance of the motor can be expressed as a function of slip only. Then, Equation (31) becomes now as a function of slip and by considering equation (15), that takes the value of r_m into account, the equivalent resistancewill be expressed as:

$$R_{eq} = \frac{S^2 r_m(r_{12s}^2 + x_{12}^2)}{k_s(r_{12s}^2 + x_{12}^2 + r_{12s} r_m)} \quad \ldots (34)$$

Specification And Design

The design process starts with the specifications for the converter performance. The minimum and maximum line voltage, the maximum output power, and the input line frequency must be specified. The design of the boost PFC converter is made on the basis of the following specifications:

- Input voltage range (rms): 85-135 V
- Line frequency (f_{line}): 50 Hz
- Output voltage (V_o): 300 V
- Maximum output power (P_{o_max}): 750 W
- Switching frequency (f_s): 30 kHz

Inner Loop: To achieve tight control, and good dynamic performance of the inductor current, the current loop must have high low-frequencies gain and wide bandwidth [23]. For the utility line frequency (f_{line}=50Hz), the gain crossover frequency (f_{ci}) should be $\gg 2f_{line}$ and may not be larger than 1/2 of the switching frequency f_s [19]. If the current loop is designed with low f_{ci} (close to $2f_{line}$), a zero-crossing distortion of the line current waveform appears due to the leading phase of the current relative to the line voltage. This leading phase is a result of control action of the current loop compensation scheme [24]. The current loop dynamic response should be designed depending on the crossover frequency f_{ci}. From equation (6), the unity gain crossover frequency can be found as

$$f_{ci} = \frac{k_{iL} k_{pi} V_{ref}}{2\pi L V_{tri}} \quad \ldots (35)$$

By determining the crossover frequency, the parameter of P-controller (k_{pi}) can be found from equation (35). The crossover frequency is chosen here to be 1/6 of the switching frequency f_s, that is $f_{ci} = 5kHz$. Values of V_{tri} and $k_{iL}$are chosen to be 3.2 and 0.1 respectively, then k_{pi} can be calculated as

$$k_{pi} = \frac{\pi L\, f_s V_{tri}}{3 k_{iL} V_{ref}} \quad \ldots (36)$$

According to (36), k_{pi} is calculated to be equals to 5.

Outer Loop: The frequency response (bode plots) for the open loop transfer function of equation (11), with different slip values, may give a good picture of the steady state and transient response performances of the outer loop. The parameters of the PI-controller may be computed to be a function of R_{eq} [25].To determine the PI Parameters, the outer-loop is compensated to satisfy the following design requirements

- Phase margin (ϕ_m)> 45°.
- Overshoot is less than 20%.
- Settling time is below 100ms.

By using the circuit parameters in table I, the open loop$G_{vOL}(s)$and the closed loop $G_{vCL}(s)$transfer function can be given as

$$G_{vOL}(s) = 0.0303 \frac{R_{eq} k_p (s + \omega_z)}{0.002 R_{eq} s^2 + 2s} \quad \ldots (37)$$

$$G_{vCL}(s) = \frac{\left(G_{vOL}(s)\right)_{\text{unity feedback}}}{1 + k_{vo}\left(G_{vOL}(s)\right)_{\text{unity feedback}}}$$

$$= \frac{1.82 R_{eq} k_p s + 1.82 R_{eq} k_p \omega_z}{0.002 R_{eq} s^2 + \left(2 + 0.0303 R_{eq} k_p\right) s + 0.0303 R_{eq} k_p \omega_z} \quad \ldots (38)$$

Using equations (37) and (38), Bode plots of the voltage loop can be computed using Matlab program and then the parameters of the PI controller can be found [25]. Fig. (9) shows the open loop frequency response and the step response of the outer loop for full load and no-load with R_{eq} represented in equations (31) and (34). In essence, equation (34) will be considered as the dependent one in the design of the controller since the system behavior is more stable and has lower overshoot than if equation (31) is used instead; especially at light load. Since the controller parameters are depending on the equivalent resistance R_{eq}, whichvaries with motor slip, this variable resistance should be maintained on a desired value that leads the controller to be a more stable. So, the loop response is examined for different load values (different values of R_{eq}) to obtain different values of the PI parameters corresponding to each R_{eq} value. This can be seenin Fig. 10, which shows that the system is stable for all values of R_{eq} (from no-load to full-load slip) but the overshoot and settling time are slightly varying according to the variation in R_{eq}. Accordingly, R_{eq} value corresponding to full-load state is to be considered in equations (37) and (38).

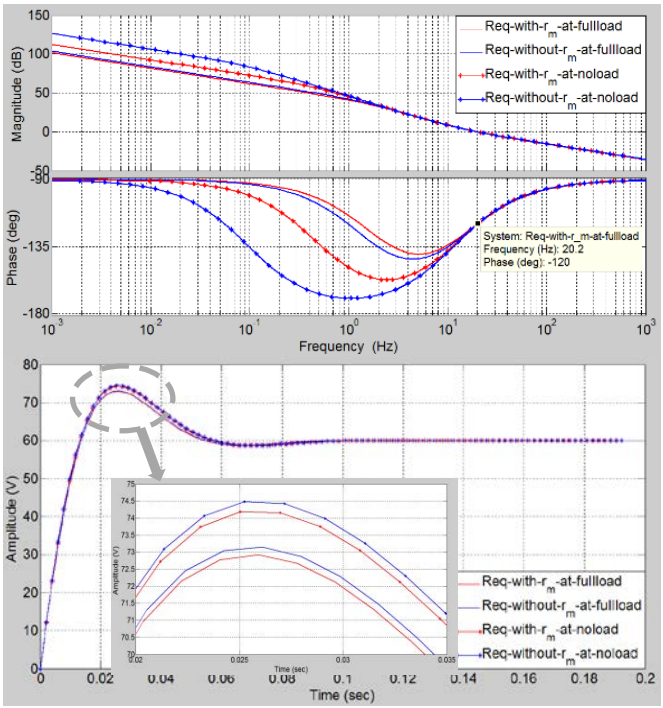

Figure. (9) Outer loop response for R_{eq} with and without r_m and$f_c = 20$Hz, upper: open loop, lower: Step response

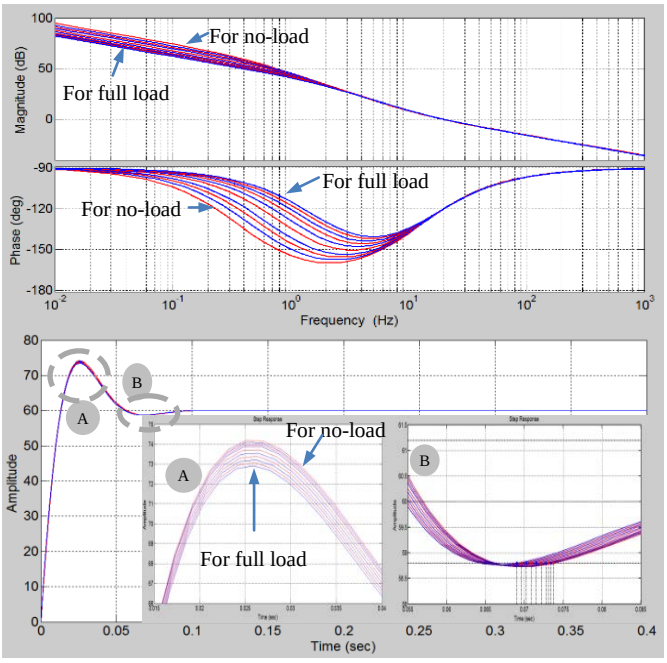

Figure. (10) Outer loop response with$\phi_m = 60°$ and$f_c = 20$Hz for different load conditions, upper: open loop, lower: Step

Now, to satisfy the design requirements, the frequency and step response of the outer loop will be examined according to the unity gain crossover frequency (f_c) and phase margin ϕ_m. First, the value of ϕ_m is to be maintained at 60°, and f_c is to be changed in the range of (3-25Hz) as in Fig (11). The figure shows that the increase in f_c improves the dynamic response (by the decrease in settling time (t_s)) but on the other hand, the peak response (maximum overshoot (M_p)) is increased. This requires a compromise between the peak response and settling time. Note that the allowable tolerance of determining t_s is considered here within 2%.

Then, as shown in Fig (12), the value of f_c is now maintained on 20Hz, and ϕ_m is to be changed in the range of $(30^\circ - 80^\circ)$. The peak response is indirectly proportional to the variation in ϕ_m but the proportionality between ϕ_m and t_s is irregular. The minimum value of t_s is obtained with $\phi_m = 70°$ and the maximum overshoot, M_p is equals 15% for $\phi_m = 70°$.

Now, to be able to determine the controller parameters, both crossover frequency f_c and phase margin ϕ_m should be determined. Concerning the phase margin, $\phi_m = 70°$ gives appropriate response ($t_s = 60ms$, $M_p = 15\%$). The crossover frequency which is compatible with the design requirements is $f_c = 15$Hz. Then, PI parameters is computed as $k_p = 4.5$ and $\omega_z = 48$ (or $k_i = 216$). The loop dynamic response is then examined for different load conditions. The open loop response in Fig. 14 shows that at full-load and at $f_c = 15$Hz, the phase angle (ϕ_p) equals -110° ($\phi_m = 70^\circ$). As the load decreases, the phase margin is slightly decreased and at no-load it reaches 64°. For the step response, the maximum overshoot M_p fluctuates between 14.5% at full-load and 20.5% at no-load. The settling time is slightly varying between 78.5msec and 76.5msec. Then, referring to Fig. (14), the bandwidth of the outer-loop is slightly varying between 19Hz and 20Hz.

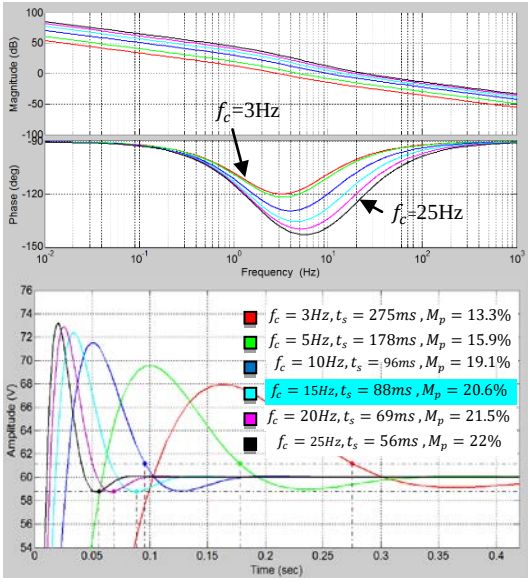

Figure.(11) Outer loop response at full-load, $\phi_m = 60°$ for different values of f_c ; upper: open loop, lower: step response

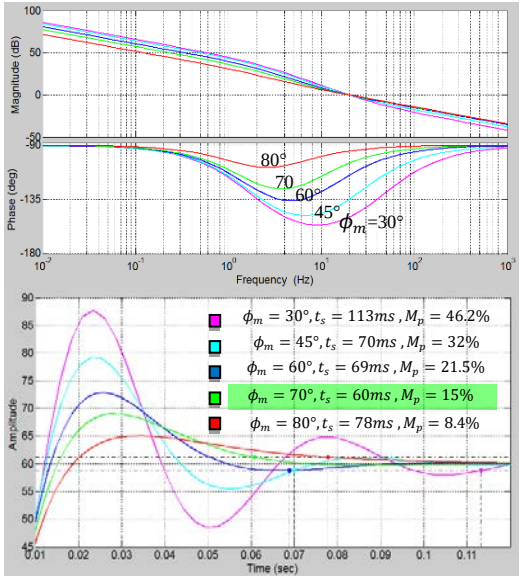

Figure.(12) Outer loop response at full-load, f_c=20Hz and for different values of ϕ_m (t_s is obtained within 2%) ; upper: open loop, lower: step response

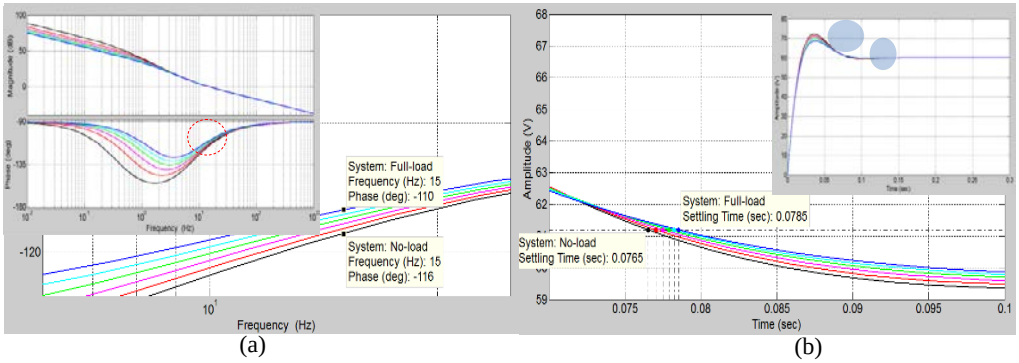

(a) (b)

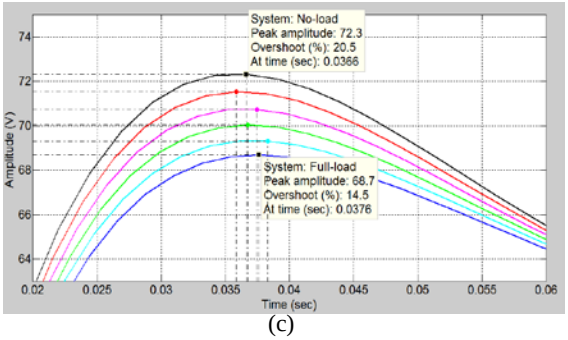

(c)

Figure.(13) Frequency response of the outer loop, with$k_p = 4.5$ and $k_i = 216$ for different load conditions; (a): open loop, (b): step response shows t_s, (c): step response shows M_p

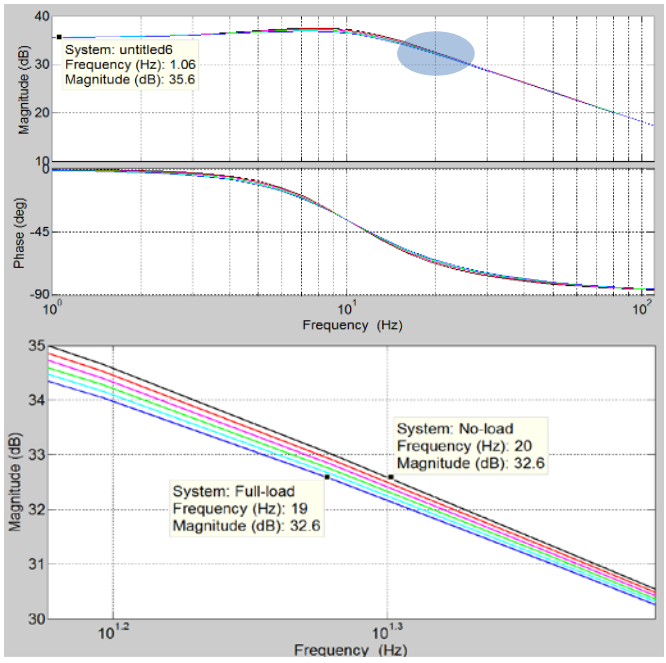

Figure.(14) Outer loop frequency response with$k_p = 4.5$ and $k_i = 216$ for different load conditions; upper: closed loop, lower: a magnified section of the magnitude in (upper) shows the loop bandwidth

System Implementation

In order to verify the designed system, a hardware prototype was built and tested. The parameters and component values of the designed system are summarized in table I and the induction motor parameters are given in table II. Fig.15 shows the laboratory prototype of the complete system including the control circuit. An Insulated Gate Bipolar Transistor (IGBT) was used as the main switch in the PFC converter, which has been operated with a switching frequency equal to 30 kHz. The induction motor (with delta connection) was loaded by a DC generator which in turn loaded by a variable resistive load.

The current controller includes the feedback P-controller and the command feedforward controller. P-controller can be simply implemented using an op-amp as shown in Fig.(15). Then the proportional control gain is calculated as:

$$G_{ib} = k_{pi} = \frac{R_{if}}{R_i} \quad \ldots (39)$$

Implementation of command feedforward controller G_{iff} is shown in Fig.(15). According to equation (3), the control signal v_{contff} can be rewritten as:

$$v_{contff} = V_{tri} - \frac{V_{tri}V_s}{V_{ref}}|sin\omega t| \quad \ldots (40)$$

Using the data of table I, equation (40) becomes:

$$v_{contff} = 3.2 - 0.01067(V_s|sin\omega t|) = 3.2 - 1.659|sin\omega t| \quad \ldots (41)$$

It is worth mentioning that the current controller output v_{cont} should be in the range between zero and peak voltage value of the carrier signal V_{tri}. In this sense, one can say that:

$$0 < \left(v_{contb} + v_{contff}\right) < 3.2\ \text{V}$$

TABLE (I)

Specifications of the designed system

parameter	value
Nominal line voltage (V_{rms})	110V
Converter output voltage (V_o)	300V
Line frequency (f_{line})	50Hz
Switching frequency (f_s)	30kHz
k_{pi}	5
k_p	4.5
k_i	216
Maximum output power (P_o)	750W
Boost inductor (L)	1.5mH
Output capacitor (C_o)	2000μF / 450V
Current sensing gain (k_{iL})	0.1
Input voltage gain (k_{vi})	0.02258
Feedforward gain (k_{vff})	0.02258
Output voltage gain (k_{vo})	0.01666

TABLE (II)

Parameters of induction motor

parameter	value
Rated power	1hp
Rated shaft speed	2860 rpm
Number of poles	2
Rated rms voltage	Δ220 V / Y380 V
Rated rms line current	Δ4.41 A / Y2.55 A
Stator resistance r_1	8.15 Ω
Rotor resistance $\acute{r}_2$	8 Ω
Stator leakage reactance	6.635 Ω
Rotor leakage reactance $\acute{x}_2$	6.635 Ω
Magnetizing resistance r_m	655.65 Ω
Magnetizing reactance x_m	232.65 Ω
Moment of inertia (J)	0.767×10^{-3} Kg.m^2
Friction coefficient	0.118×10^{-3}N.m.s/rad

To achieve this, a zener diode, with a reverse voltage equal to the peak voltage value of the carrier signal V_{tri}, can be used as shown in Fig.(15). For the voltage controller, a typical analogue proportional-integral controller schematic is used as shown in Fig. 15. By using the PI parameters $k_p = 4.5$ and $k_i = 216$, the components of the PI-controller can be selected using the following equations:

$$k_p = \frac{R_{vf}}{R_v} \quad \ldots (42)$$

$$k_i = \frac{1}{R_v C_{vf}} \quad \ldots (43)$$

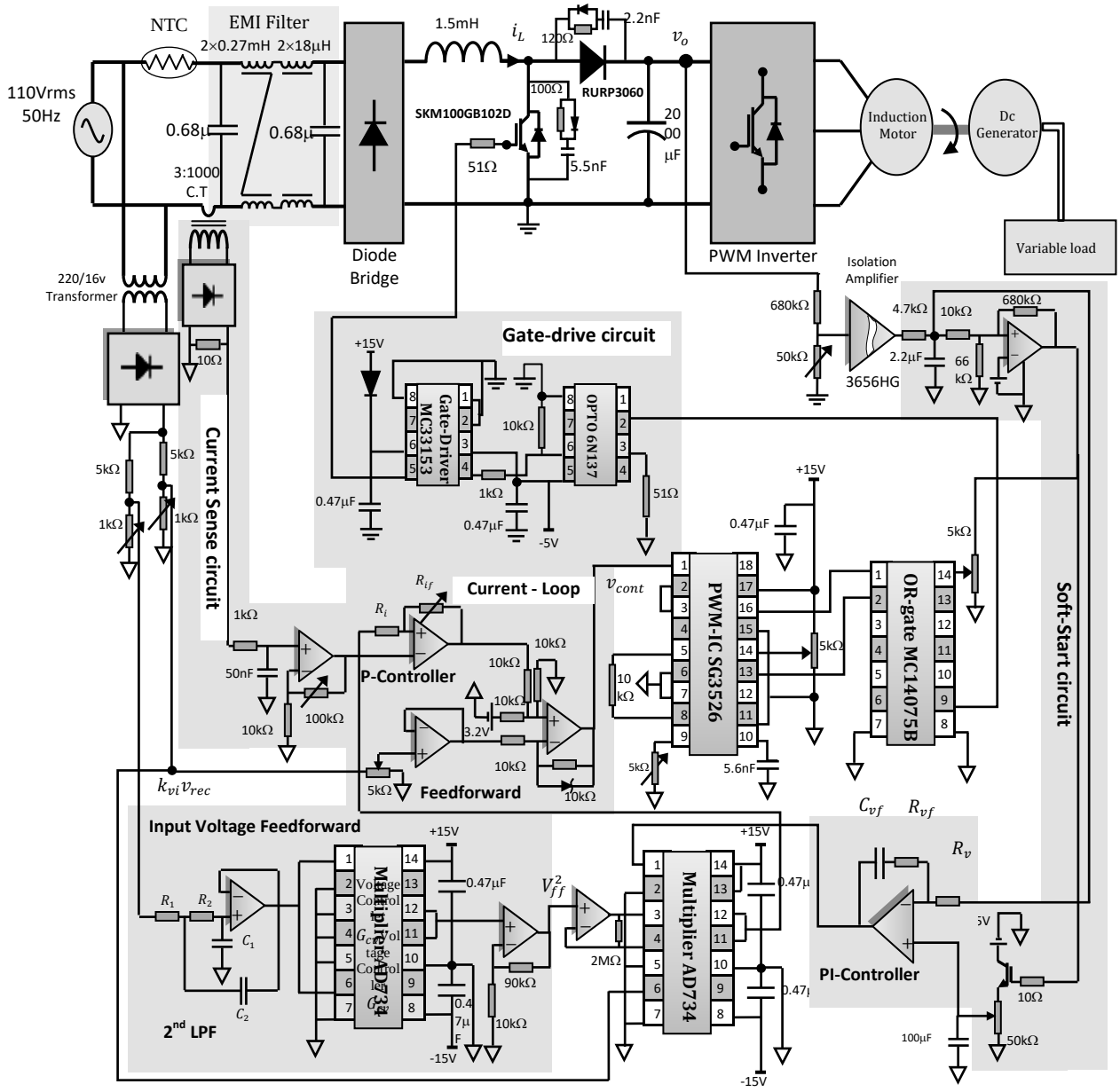

Figure.(15) Full schematic diagram of the boost PFC converter circuit

At the instant of starting, with no initial voltage across C_o, boost converter suffers from a large transient inrush current due to the low input impedance of the converter. This inrush current causes excessive stress on boost components, and may causes saturation in the inductor. Another issue is related to the starting that the control circuit is not in its normal working condition but in its full rating. As a result, the switching on-state persists for relatively long periods, which can damage the main switch. These issues can be solved by:

- Using inrush current limiter
- Using soft-start circuit
- Turning-off the IGBT until the capacitor is approximately fully charged.

Negative Temperature Coefficient (NTC) thermistor, with 10Ω value, is used here as inrush current limiter to reduce the inrush current caused by the output capacitor. For the other two solutions, a start-up circuit, shown in Fig. (15), is suggested. The soft-start is done by gradually increasing the reference voltage V_{ref} of the voltage controller through a delay function. To turns-off the IGBT at starting, a hysteresis band comparator is used to shutting-down the OR-gate until the voltage across the output capacitor reaches 130V.

Experimental Results

At steady state, Fig. (16) shows the input line current of the PFC Boost circuit with 110V (rms) input line voltage and the induction motor is fully loaded. A near sinusoidal input current is obtained with the Total Harmonic Distortion of the input current (THD_i) equals to 2% and the PF is found to be (0.997). The harmonic spectrum of the input line current is shown in Fig. (17).

Fig. (18) shows the output voltage of the boost converter at starting with the use of the start-up circuit. At the instant of start-up, the main switch (IGBT) is in the off-state for approximately 1sec and then the soft-start circuit delays the reference voltage of the voltage controller with about 1.5sec to reach its steady state. The inrush current is found to be 33A (peak) as shown in Fig.(18b). The measured harmonic components of the line input current given in Fig.(19) is compared with the IEC 61000-3-2 Class A standard. The figure shows that the measured harmonic components (rms) of the input current (I_{n_rms}), expressed as a percent of the rms fundamental current (I_{1_rms}), are much lower than those of the IEC limits.

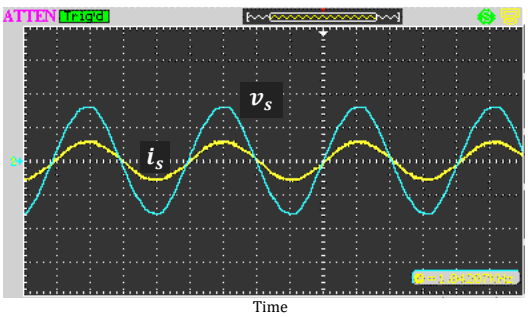

Figure.(16) Steady state waveforms of input current i_s and input voltage$v_s$at full-load and$f_{inv} = 50Hz$, i_s (20A/div), v_s (100V/div)

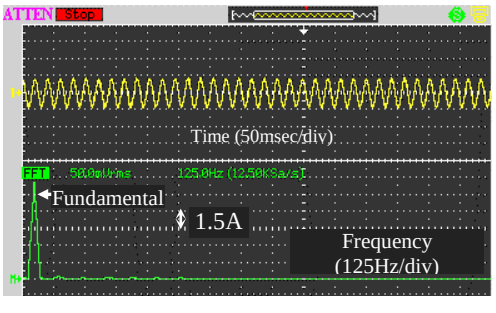

Figure.(17) Harmonic spectrum of the measured input line current (rms) at full-load

Fig. (20) shows the boost PFC converter performance in terms of PF, THD_i, and converter efficiency when the output power P_o varies from 200W to 750W and with f_{inv} equal to 50Hz. The recorded input PF is found to be near unity and the THD of input current is complied with IEC 61000-3-2 regulation. In spite of the hard switching operation, the single-phase boost PFC shows good performance in terms of efficiency. The system is tested with 85V and 135V input voltage at full-load operation. THDi and PF are found to be 5.4% and 0.988 respectively for 85V input voltage. For 135V, THDi and PF are found to be 3.2% and 0.991 respectively.

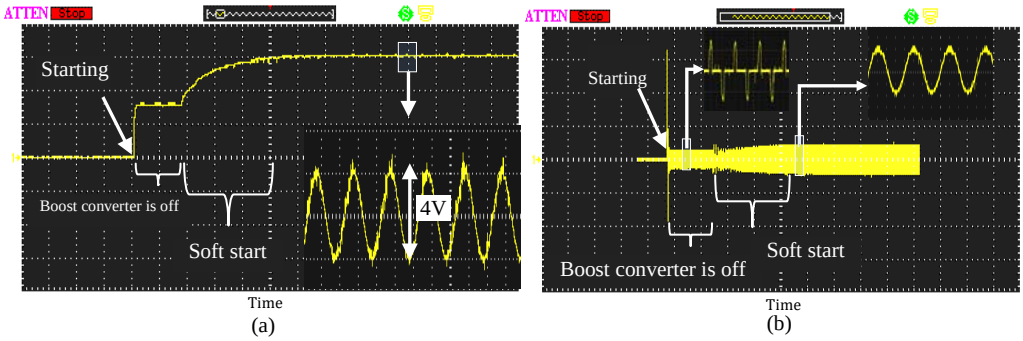

Figure. (18) Output voltage v_o and input current i_s of the boost converter at starting: (a) v_o (100V/div); (b) i_s(10A/div)

Fig. (21) shows the measured equivalent resistance ($R_{eq} = V_o/I_o$), as a function of motor slip for different load condition with $f_{inv} = 50Hz$, compared with the computed R_{eq} in both equation (31) and (34) which have been derived in section 3. It is clear from this figure that the measured R_{eq} coincides with that of equation (34) more than that from equation (31). This consolidates the choice of equation (34) in the voltage loop design and validates the derivation of R_{eq}.

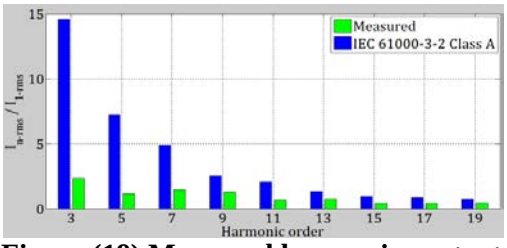

Figure.(19) Measured harmonic content of the input current at full-load versus IEC 61000-3-2 Class A limits

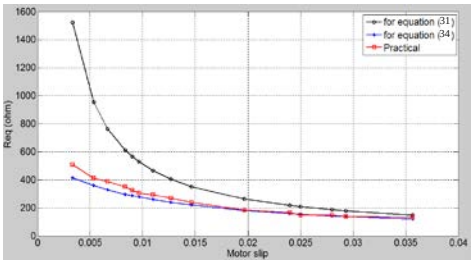

Figure. (21) R_{eq} vs. motor slip at f_{inv} = 50Hz

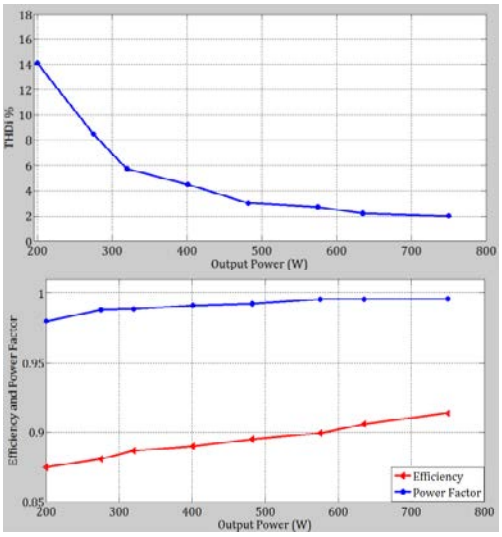

Figure.(20) PFC converter performance with respect to the output power; upper: THD_i vs. P_o, lower: efficiency and PF vs.

Figure. (22) and Fig. (23) show the same considerations as in Figure. (21) but each curve represents the equivalent resistance when the motor is running with different load condition. The inverter frequency is changed from 50-25Hz in steps to obtain different cases. Fig. (22) shows that the computed R_{eq} from equation (31) diverges from the measured one in all operating frequency ranges. Fig. (23) shows that the computed R_{eq} of equation (34) is close to the measured R_{eq}, when f_{inv} is in the range of 50-40Hz, and begins to diverge (gradually) from it when f_{inv} is below 40Hz.

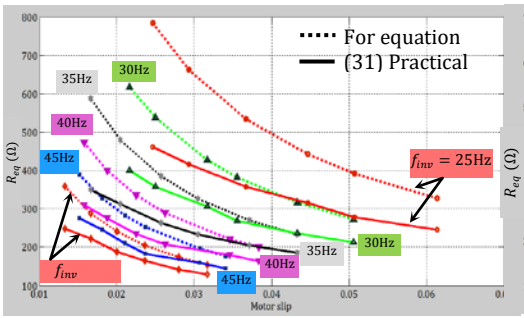

Figure. (22) R_{eq} (from equation (31)) vs. motor slip for different load condition with f_{inv}varied from 50Hz to 25Hz

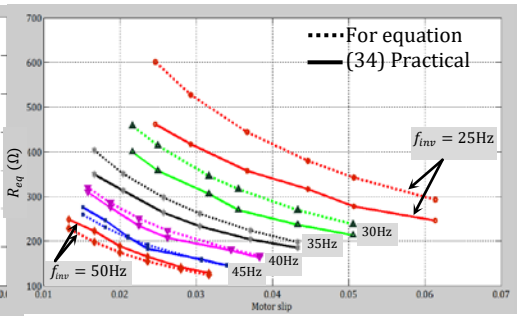

Figure. (23) R_{eq} (from equation (34)) vs. motor slip for different load condition with f_{inv}varied from 50Hz to 25Hz

Good agreements between the evaluated and the measured equivalent resistance of the inverter-motor system have been obtained when the motor is operated at the rated frequency and rated voltage (50Hz, 220V). However, when operating below the motor rating under *v/f* control at a constant load operation, the evaluated equivalent resistance has been gradually diverged from the measured one. This may be attributed to one (or both) of the following:

- The assumption of sinusoidal inverter: operation of the inverter with low frequency and low voltage increases the harmonics in the inverter voltage, and hence, the measured (averaged) current drawn by the boost converter is larger. Accordingly, a lower value of the measured equivalent resistance is obtained compared with the calculated value.
- The assumption of lossless inverter: with low frequency operation, inverter losses are increased (the efficiency decreased). It has been found (in section 3) that the equivalent resistance is in direct proportion with the inverter efficiency.

CONCLUSION

In this paper, a systematic analysis and design of a single-phase boost PFC converter supplying an inverter-motor drive system has been presented. The inverter-motor system has been analyzed as a load across the converter. It has been found that the equivalent of this load system, seen by the converter, can be represented as a variable resistive load that is varying as a function of the motor slip. The analysis shows that by finding this equivalent resistance, the design of the PFC controller becomes easier and the control parameters can be designed according to frequency response analysis to ensure system stability without the use of trial and error method. Experimental prototype has been used to verify the analysis of the proposed method. The experimental results showed good agreement with the analytical results.

REFERENCES

[1] Electromagnetic Compatibility (EMC)–Part 3: Limits-Section2: Limits for Harmonic Current Emissions (Equipment Input Current <16 A per-Phase), IEC 61000-3-2, 1998.

[2] S. K. Sul and T. A. Lipo, "Design and performance of a high frequency link induction motor drive operating at unity power factor," IEEE Trans. Ind. Appl., vol. 26, no. 3, pp. 434–440,May/Jun. 1990.

[3] K. Thiyagarajah, V. T. Ranganathan, and B. S. Ramakrishna lyengar, "A High Switching Frequency IGBT PWM Rectifier/inverter System for AC Motor Drives Operating from Single Phase Supply," IEEE Trans. on Power Electron., vol. 6, no.4, pp. 576-584, October 1991.

[4] A. Consoli, M. Cacciato, A. Testa, and F. Gennaro, "Single chip integration for motor drive converters with power factor capability", IEEE Trans. Power Electron., vol. 19, no. 6, pp. 1372–1379, Nov. 2004.

[5] D.-C. Lee and Y.-S. Kim, "Control of single-phase-to-three-phase AC/DC/AC PWM converters for induction motor drives," IEEE Trans. Ind. Electron., vol. 54, no. 2, pp. 797–804, Apr. 2007.

[6] J.-ichiItoh and N. Ohtani, "Square-Wave Operation for a Single-Phase-PFC Three-Phase Motor Drive System Without a Reactor," IEEE Trans. Ind. Appl., vol. 47, no. 2, pp. 805–811, Mar./Apr. 2011.

[7] S. Singh, and B. Singh, "A Voltage-Controlled PFC Cuk Converter-Based PMBLDCM Drive for Air-Conditioners," IEEE Trans. Ind. Appl., vol. 48, no. 2, pp. 832–838, Mar./Apr. 2012.

[8] M. Morimoto, K. Sumito, S. Sato, K. Oshitani, M. Ishida, S. Okuma, " High Efficiency, Unity Power Factor VVVF Drive System of an Induction Motor," IEEE Trans. Power Electron., vol. 6, no. 3, pp. 498–503, Jul. 1991.

[9] J. C. Liao and S. N. Yeh, "A novel instantaneous power control strategy and analytic model for integrated rectifier/inverter systems," IEEE Trans. Power Electron., vol. 15, no. 6, pp. 996–1006, Nov. 2000.

[10] J.R. Wells, B.M. Nee, M. Amrhein, P.T. Krein, P.L. Chapman, "Low-Cost Single-Phase Powered Induction Machine Drive for Residential Applications," in Proc. Applied Power Electronics Conference and Exposition, IEEE, APEC, 2004, pp. 1579–1583.

[11] M. Bhardwaj, S. Choudhury, B. Akin, "Digital Control of Two Phase Interleaved PFC and Motor Drive using MCU with CLA" IEEE, APEC, Fort Worth, 2011, pp. 384–389.

[12] J. Adabi, A.A. Boora, F. Zare, A. Nami, A. Ghosh, and F. Blaabjerg, "Common-mode voltage reduction in a motor drive system with a power factor correction," IET Power Electron., Vol. 5, Iss. 3, pp. 366–375, 2012.

[13] M. Bellar. B.K. Lee. B. Fahimi. and M. Ehsani. "An AC Motor Drive with Power Factor Control for Low Cost Applications", in Proc. IEEE-APEC. vol. 1. 4-8 March 2001, pp. 601-607.

[14] J.-Y. Chai and C.-M. Liaw, "Development of a Switched-Reluctance Motor Drive with PFC Front End," IEEE Trans. Energy Convers., vol. 24, no. 1, pp. 30–42, Mar. 2009.

[15] G. Chu, C. K. Tse, S. C. Wong, and S.-C. Tan, "A Unified Approach for the Derivation of Robust Control for Boost PFC Converters," IEEE Trans. Power Electron., vol. 24, no. 11, pp. 2531–2544, Nov. 2009.

[16] K. P. Louganski and J. S. Lai, "Current phase lead compensation in single-phase PFC boost converters with a reduced switching frequency to line frequency ratio," IEEE Trans. Power Electron., vol. 22, no. 1, pp. 113–119, Jan. 2007.
[17] O. Garcia, J. A. Cobos, R. Prieto, P. Alou, and J. Uceda, "Single phase power factor correction: A survey," IEEE Trans. Power Electron., vol. 18, no. 3, pp. 749–755, May 2003.
[18] S. Wall and R. Jackson, "Fast controller design for single-phase power-factor-correction systems," IEEE Trans. Ind. Electron., vol. 44, no. 5, pp. 654–660, Oct. 1997.
[19] H. C. Chen, S. H. Li, and C. M. Liaw, "Switch-mode rectifier with digital robust ripple compensation and current waveform controls," IEEE Trans. Power Electron., vol. 19, no. 2, pp. 560-566, Mar. 2004.
[20] R. Ghosh and G. Narayanan, "Generalized feedforward control of single-phase PWM rectifiers using disturbance observers," IEEE Trans. Ind. Electron., vol. 54, no. 2, pp. 984–993, Apr. 2007.
[21] H.-C. Chen, H.-Yi Li, and R.-S. Yang, "Phase Feedforward Control for Single-Phase Boost-Type SMR," IEEE Trans. Power Electron., vol. 24, no. 5, pp. 1428-1432, May. 2009.
[22] C. K. Tse, "Circuit Theory and Design of Power Factor Correction Power Supplies," IEEE Distinguished Lecture 2005, Circuits and Systems.
[23] P. C. Todd, "UC3854 Controlled, Power Factor Correction Circuit Design," Unitrode Corp., Merrimack, NH, Appl. Note U-134, pp. 3-269–3-288, 1999.
[24] J. Sun, "On the zero-crossing distortion in single-phase PFC converter," IEEE Trans. Power Electron., vol. 19, no. 3, pp. 685–692, May 2004.
[25] R. F. Abbas, "Single-Phase Boost Power Factor Corrected Converter for Induction Motor Drive," M.Sc. Thesis, Baghdad University, Baghdad, 2012.
[26] M.G. Say, "Alternating current machines," Pitman, London, 1984.
[27] D. Fewson, "Introduction to Power Electronics," Arnold, London, 1998.